

## Chapter 19

# Nuclear resonant inelastic X-ray scattering and synchrotron Mössbauer spectroscopy with laser-heated diamond anvil cells

Jung-Fu Lin, Wolfgang Sturhahn, Jiyong Zhao,  
Guoyin Shen, Ho-kwang Mao and Russell J. Hemley

### Abstract

The laser-heated diamond anvil cell (LHDAC) technique is a uniquely powerful method for generating the ultrahigh static pressures and temperatures ( $P > 100$  GPa and  $T > 3000$  K) found deep within planetary interiors. Here we show that the LHDAC technique can be used in conjunction with nuclear resonant inelastic X-ray scattering and synchrotron Mössbauer spectroscopy for studying magnetic, elastic, thermodynamic, and vibrational properties of  $^{57}\text{Fe}$ -containing materials under high pressures and temperatures. A Nd:YLF laser, operating in continuous donut mode ( $\text{TEM}_{01}$ ), has been used to heat a sample of  $^{57}\text{Fe}$ -enriched hematite ( $\text{Fe}_2\text{O}_3$ ) and iron from both sides of a diamond cell. Temperatures of the laser-heated sample are measured by means of spectroradiometry and the detailed balance principle of the energy spectra. The detailed balance principle applied to the inelastic X-ray scattering spectra provides absolute temperatures of the laser-heated sample. When the sample was heated evenly on both sides, these temperatures were in very good agreement with values determined from the thermal radiation spectra fitted to the Planck radiation function. Synchrotron Mössbauer spectra and partial phonon density of states (PDOS) of  $\text{Fe}_2\text{O}_3$  have been obtained with these techniques up to 24 GPa and 1400 K, providing rich information for understanding physical properties of the sample under high pressures and temperatures. Time spectra of the synchrotron Mössbauer spectroscopy at 10 and 24 GPa upon laser heating reveal that  $\text{Fe}_2\text{O}_3$  undergoes a magnetic-to-nonmagnetic transition at 900 ( $\pm 100$ ) K and 1000 ( $\pm 100$ ) K, respectively, from a room-temperature magnetic state to a high-temperature nonmagnetic state. The PDOS of  $\text{Fe}_2\text{O}_3$  are shifted to lower energies at 1400 K, indicating the softening of the lattice vibrations at high temperatures. This study demonstrates a new arsenal of *in situ* probes to study magnetic, vibrational, elastic, and thermodynamic properties of  $^{57}\text{Fe}$ -containing materials, such as metallic Fe, Fe alloys, and iron-bearing oxides and silicates [(Mg,Fe)O and (Mg,Fe)SiO<sub>3</sub>], in the Earth's interior.

### 1. Introduction

Since the birth of the laser-heated diamond anvil cell (LHDAC) in the late 1960s (Ming and Bassett, 1974; Bassett, 2001), the LHDAC technique has been widely used with *in situ* X-ray diffraction, melting point studies, phase equilibrium studies, and chemical analyses of quenched samples (Boehler, 1986; Shen et al., 1998; Boehler and Chopelas, 1991; Lazor et al., 1993; Dewaele et al., 2000; Shen et al., 2001). *In situ* X-ray diffraction studies of materials deep in the Earth's mantle and core have advanced our understanding of the possible mineralogy and composition of the Earth's interior (Hemley et al., 2000).

Recently, the LHDAC technique has also been used with *in situ* high-pressure and high-temperature Raman spectroscopy to study vibrational properties of materials under these conditions (Lin et al., 2004a; Santoro et al., 2004). These studies have yielded data on the phase diagram, equation of state (EOS), elasticity, composition, and melting curve of planetary materials. However, important physical properties of planetary materials, such as magnetic, elastic, and thermodynamic properties under simultaneous high pressure and temperature conditions, remain to be explored with other techniques.

The nuclear resonant inelastic X-ray scattering (NRIXS) technique provides a direct probe of the phonon density of states (DOS) of a resonant isotope (Seto et al., 1995; Sturhahn et al., 1995, 1998; Lübbbers et al., 1999a; Ruffer and Chumakov, 2000; Sturhahn, 2000; Alp et al., 2001; Sturhahn, 2004), e.g. using the 14.4125 keV transition of  $^{57}\text{Fe}$ , whereas the synchrotron Mössbauer spectroscopy (SMS) technique probes the magnetic properties of a sample (Hastings et al., 1991; Lübbbers et al., 1999b). The most suitable nuclear resonant isotope is  $^{57}\text{Fe}$ , and iron-containing materials, such as hcp-Fe, magnesiowüstite  $[(\text{Mg},\text{Fe})\text{O}]$ , and silicate perovskite  $[(\text{Mg},\text{Fe})\text{SiO}_3]$ , are of tremendous interest in mineral physics. The NRIXS technique is truly unique for the study of lattice vibrations because the NRIXS signals only originate from particular nuclei with a complete isotope selectivity, and materials surrounding the sample that do not contain resonant nuclei produce no unwanted background, permitting detailed studies of iron-containing materials in a diamond anvil cell (DAC). For pure  $^{57}\text{Fe}$  sample, one can obtain full phonon DOS and derive elastic, thermodynamic, and vibrational parameters fully contributed from the  $^{57}\text{Fe}$  sample. For  $^{57}\text{Fe}$ -containing materials, such as magnesiowüstite  $[(\text{Mg},\text{Fe})\text{O}]$  and silicate perovskite  $[(\text{Mg},\text{Fe})\text{SiO}_3]$ , a partial DOS is obtained from the contribution of the Fe sublattice. Physical parameters derived from the partial DOS only represent the contribution of the Fe sublattice vibrations, and theoretical calculations may be needed to complement experimental results.

The NRIXS and SMS techniques have been used to study elastic, magnetic, thermodynamic, and vibrational properties of hexagonal close-packed (hcp) Fe at high pressures (Lübbbers et al., 2000; Mao et al., 2001; Gieffers et al., 2002; Struzhkin et al., 2004), hcp-Fe to 29 GPa and 920 K by wire heating (Shen et al., 2004), Fe–Ni, Fe–Si, Fe–S, and Fe–H alloys (Lin et al., 2003; Lin et al., 2004b; Mao et al., 2004), iron valencies in  $(\text{Mg},\text{Fe})\text{SiO}_3$  perovskite to 120 GPa (Jackson et al., 2005), and high-pressure and/or high-temperature study of magnetism (Lübbbers et al., 1999b; Rupprecht et al., 2002; Pasternak et al., 2004), providing important information on the physical properties of Fe and its alloys, such as compressional wave velocity ( $V_p$ ), shear wave velocity ( $V_s$ ), and shear modulus ( $G$ ) under high pressures. However, NRIXS and SMS studies under the pressure and temperature conditions of the Earth's interior remain to be explored, mainly due to the weak NRIXS signals, long data collecting time, and long-term laser heating stability. The typical collecting time for a meaningful NRIXS spectrum of a metallic  $^{57}\text{Fe}$  in a DAC at the 3ID beamline of the Advanced Photon Source (APS), Argonne National Laboratory (ANL) is at least 4–6 h, suggesting that a LHDAC system that provides stable heating conditions on the order of hours needs to be built for such studies to be successful. Moreover, the use of a high-resolution monochromator with meV bandwidth and avalanche photodiode detectors (APD) requires extremely sensitive hutch-temperature control in the mK range, complicating the combination of the LHDAC and NRIXS techniques.

Here we describe the application of the LHDAC technique in NRIXS and SMS studies using hematite ( $\text{Fe}_2\text{O}_3$ ) as an example. The SMS spectra and partial phonon density of states (PDOS) of hematite have been obtained with these techniques up to 24 GPa and 1400 K. Time spectra were evaluated with the CONUSS (coherent nuclear resonant scattering by single crystals) programs to permit deviation of magnetic hyperfine parameters, whereas elastic, thermodynamic, and vibrational parameters were derived by evaluating the energy spectra using the PHOENIX (phonon excitation by nuclear inelastic scattering of X-rays) programs (Sturhahn, 2000).

## 2. Laser-heating system set-up and sample configuration

We have built a double-sided laser-heating system at sector 3 of the APS, ANL for NRIXS and SMS studies of materials under high pressures and high temperatures (Figs 1 and 2). A Nd:YLF laser, operating in continuous donut mode ( $\text{TEM}_{01}$ ), was used to heat a sample of  $^{57}\text{Fe}$ -enriched hematite ( $\text{Fe}_2\text{O}_3$ , 96% enrichment or better) from both sides of a DAC (Shen et al., 2001). Flat diamonds with a culet of 400  $\mu\text{m}$  were used to pre-indent a beryllium gasket to a thickness of 30  $\mu\text{m}$ . A hole with a 150  $\mu\text{m}$  diameter was drilled in the indented area and filled with a sandwich configuration of hematite sample and dried NaCl, for the thermal insulator and pressure medium, on both sides of the sample (Fig. 2). During the experiments, the diameter of the laser beam at the sample position was about 40  $\mu\text{m}$ . Greybody temperatures were determined by fitting the thermal radiation spectrum between 670 and 830 nm to the Planck radiation function (Shen et al., 2001). We also measured temperatures of the laser-heated sample by the temperature-dependent intensity asymmetry of the energy spectra based on the detailed balance principle (Lin et al., 2004c; Shen et al., 2004). The detailed designs and experimental procedures of the laser-heating system are similar to a system installed at GSECARS of the APS (Shen et al., 2001; Lin et al., 2004c). A back-illuminated CCD enabled us to measure temperatures above 1000 K. Pressures were measured before and after laser heating from rubies placed in the NaCl medium using the ruby pressure scale (Mao et al., 1978).

## 3. NRIXS and SMS experiments

The NRIXS experiments were conducted using a high-resolution monochromator with 1 meV energy bandwidth. The high-energy resolution is essential for deriving accurate Debye sound velocities ( $V_D$ ) from the DOS (the Debye parabola is best constrained at the lower energy limit) (Hu et al., 2003; Sturhahn, 2004). Energy spectra were obtained by tuning the X-ray energy ( $\pm 70$  meV) around the nuclear transition energy of 14.4125 keV and collecting the Fe K-fluorescence radiation that was emitted with time delay relative to the incident X-ray pulses. The fluorescence radiation was collected by three APDs, and the fourth APD along the beam was used to record synchrotron Mössbauer spectra in which the incident X-ray energy was fixed at 14.4125 keV (Figs 1 and 2) (Sturhahn, 2004). The diameter of the focused X-ray beam was 6–7  $\mu\text{m}$  (FWHM) in both vertical and horizontal directions; the small beam size insured that the signal from the sample was only measured within the laser-heated spot of 40  $\mu\text{m}$  (Fig. 2). The beam size was measured by scanning a

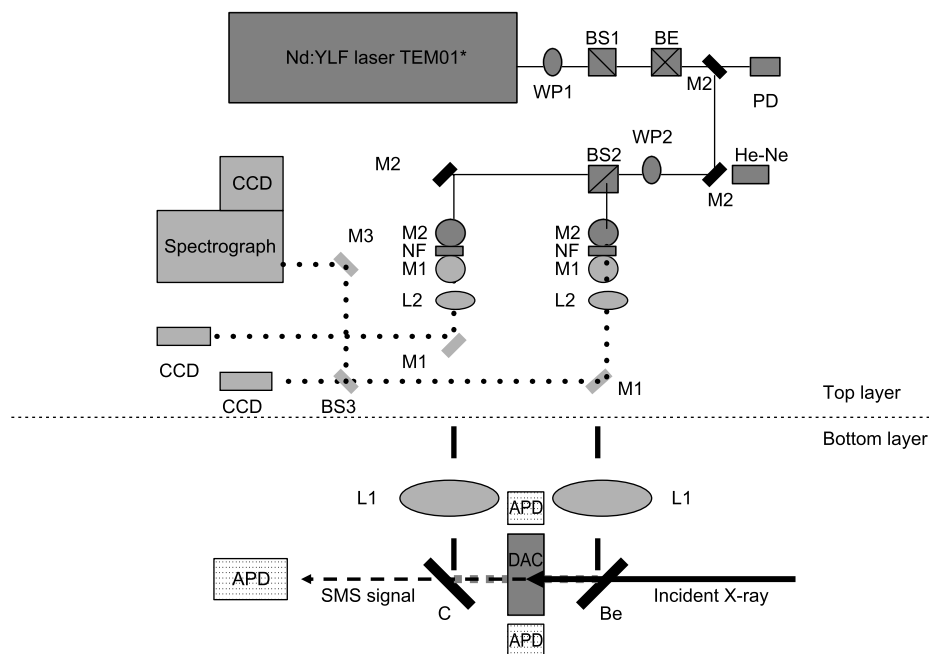


*Figure 1.* Schematic of the double-sided laser heating system combined with the NRIXS technique at sector 3 of the Advanced Photon Source. A continuous wave Nd:YLF laser beam in TEM<sub>01</sub> mode (donut mode) with a maximum output power of 80 W was regulated by the wave plate (WP1) and polarized beam splitter (BS1). The laser beam was split into two beams by the second wave plate and polarized beam splitter (WP2 and BS2), which were also used to balance the laser power between the upstream and downstream sides. The laser beams were focused onto  $\sim 40\ \mu\text{m}$  at the sample. An upstream beryllium mirror coated with gold and a downstream carbon mirror coated with silver were used to guide the laser beam and to reflect the thermal radiation. The wide-angle DAC was constantly cooled by the attached cooling plates insuring the stability of the cell temperature and the sample position during laser heating. The temperature of the DAC stays below than 310 K during data collection, which ensures mechanical stability. The front entrance of each APD detector was covered with a thin Be window to protect the device from light. The Fe K-fluorescence radiation was collected by three APDs surrounding the DAC. The fourth APD in transmission was used to record the SMS signal. Thin black line: YLF laser; thick black line: incident X-rays; dotted grey line: white light/thermal emission; dash/dotted line: laser and white light path. WP and BS: wave plate and polarized beamsplitter to regulate the Nd:YLF laser; BE: beam expander; M2: dichroic laser mirror reflects at least 99.5% of the YLF laser and transmits more than 90% of the visible light; PD: photodiode; He-Ne: He-Ne laser for alignment; M1: aluminum-coated mirror; NF: notch filter; L1: laser lens; L2: achromatic lens; BS3: 50/50 beam splitter.

Si edge (coated with Cr) across the X-ray beam in both the horizontal and vertical directions while collecting Cr K fluorescence with a Si(Li) detector. The counting time for each spectrum was 45 min, and between 10–15 spectra were collected at the same pressure and temperature conditions and added. At present a total collection time of up to 10 h is required to have good statistical accuracy of the energy spectra. In fact, continuously stable laser heating of the sample in a DAC for more than half a day has been achieved in this study. Elastic, thermodynamic, and vibrational parameters of the measured sample under high pressures were derived by evaluating the energy spectra

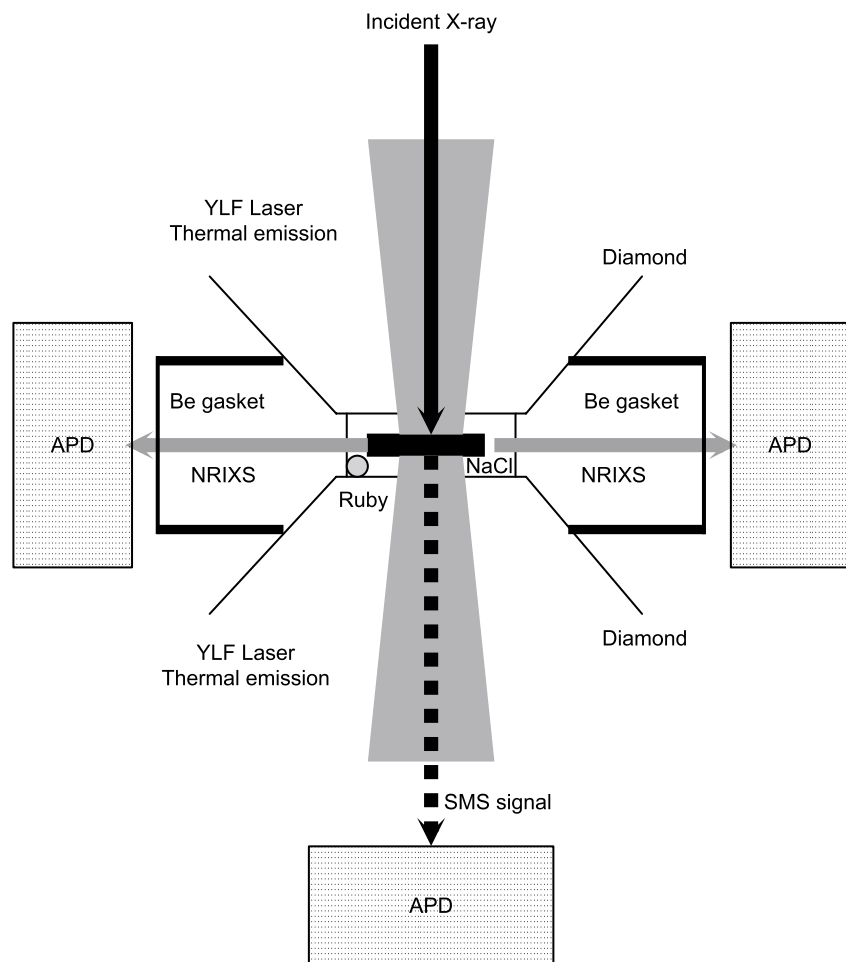


*Figure 2.* Schematic of the LHDAC in the NRIXS and SMS experiments. The YLF laser beam is focused to  $40\ \mu\text{m}$  onto the sample surface. The fluorescence radiation was collected by three APD, and the fourth APD along the beam was used to record synchrotron Mössbauer spectra (Fig. 1) (Sturhahn, 2004). The diameter of the focused X-ray beam was less than  $10\ \mu\text{m}$  (FWHM); the small beam size insured that the signal from the sample was only measured within the laser-heated spot of  $40\ \mu\text{m}$ . Small ruby chips were placed in the sample chamber as a pressure calibrant. NaCl was used as thermal insulating layers.

using the PHOENIX (phonon excitation by nuclear inelastic scattering of X-rays) programs (Sturhahn, 2000).

The collection time of the SMS for each time spectrum was approximately 30 min. In the SMS experiments, the time spectrum is a collection of events that reveal the time span between arrival of the synchrotron radiation pulses and arrival of a scattered photon. The time spectra were recorded by an APD in the forward direction in which the incident X-ray energy was fixed at  $14.4125\ \text{keV}$  (Figs 1 and 2). Time spectra can be evaluated with the CONUSS (coherent nuclear resonant scattering by single crystals) programs to permit deviation of magnetic hyperfine parameters (Sturhahn, 2000; Lin et al., 2004b).

#### 4. Temperature measurements based on the detailed balance principle

We have measured temperatures of the laser-heated sample by two different methods: spectroradiometry (Heinz and Jeanloz, 1987; Shen et al., 2001) and temperature-dependent intensity asymmetry of the energy spectra based on the detailed balance principle. Here NRIXS spectra of hematite were measured up to 24 GPa and 1400 K, and we used the detailed balance principle to determine the average temperature of the laser-heated sample. In Figure 3, the side band at positive energies represents phonon creation, whereas the side band at negative energy arises from phonon annihilation. The intensity ratio of phonon creation to phonon annihilation is low at 300 K; this intensity imbalance is reduced with increasing temperature due to the rising thermal population of the upper energy level of the phonons. The asymmetry of the NRIXS spectra is independent of sample properties other than temperature and is given by the Boltzmann factor,  $\exp[-E/k_{\text{B}}T]$  with the Boltzmann constant  $k_{\text{B}}$ , temperature  $T$ , and energy  $E$ . Therefore, the intensity ratio is given by

$$\frac{I(E)}{I(-E)} = e^{\frac{E}{k_{\text{B}}T}} \quad (1)$$

where  $I(E)$  is the intensity of the phonon creation and  $I(-E)$  is the phonon annihilation. Each pair of measured intensities  $I(\pm E)$ , where  $E = 0$  corresponds to the nuclear transition energy of 14.4125 keV (the band width is 4.66 neV), gives a temperature value. The average temperature of the laser-heated sample is then determined by integrating all energy pairs from the energy range of 5–70 meV using the following equation:

$$\int I(E)dE = \int e^{\frac{E}{k_{\text{B}}T}} I(-E)dE \quad (2)$$

The average that is determined gives the sample temperature within the statistical accuracy of the spectra, which in our case is 5–10%. Error analyses of the temperature determination based on the principle of the detailed balance principle show that the uncertainty in temperature increases at very low temperatures, where the intensity of the phonon annihilation is too weak, and also at ultrahigh temperatures, where the intensity ratio is almost equal to 1 (Shen et al., 2004). However, the counting rate is also high at higher temperatures which, in turn, would improve the statistical accuracy. When the sample was heated evenly on both sides, these temperatures showed very good agreement with temperatures obtained from the spectroradiometric method (Lin et al., 2004c). The spectroradiometric method for temperature measurement in the LHDAC has been widely used to study planetary materials, but the accuracy of obtained temperature values has been debated (Heinz and Jeanloz, 1987). The absolute temperature determination using the energy spectra and the detailed balance principle independently confirm the validity of temperatures determined from the Planck radiation law in LHDAC experiments. However, temperature-dependent spectral emissivity should be taken into account in the spectroradiometric method at higher temperatures where the spectral emissivity may be affected by high temperature (Heinz and Jeanloz, 1987; Shen et al., 2001; Lin et al., 2004c).

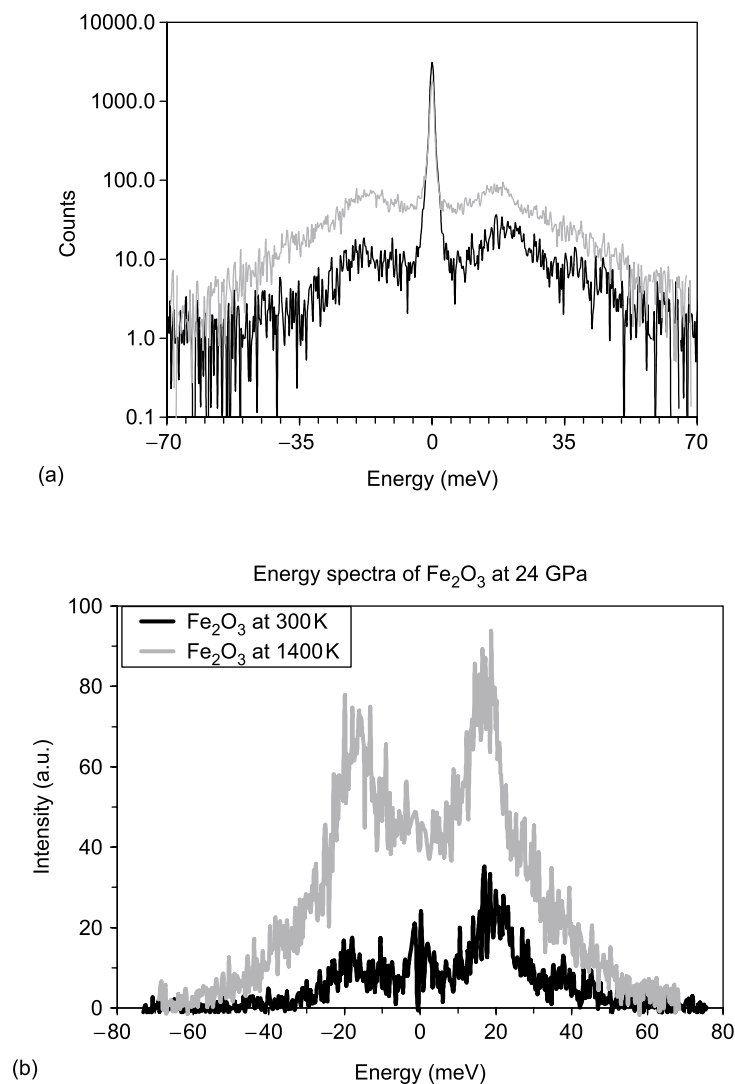


*Figure 3.* Energy spectra of hematite at 24 ( $\pm 1.2$ ) GPa and 300 K (black curve) and 24 ( $\pm 1.2$ ) GPa and 1400 K ( $\pm 100$ ) (grey curve) before and after the elastic peak at zero energy was removed (a, b). (a) is in log scale. Energy zero corresponds to the nuclear transition energy of 14.4125 keV. The counting time for each spectrum was approximately 10 h. Negative/positive energies indicate net phonon annihilation/creation. At 300 K (black curve) the probability of phonon annihilation is clearly lower than that for phonon creation. This imbalance is reduced at higher temperature (grey curve) because phonon creation and annihilation probabilities grow equally fast with temperature. The asymmetry of these spectra was used to determine the average temperature of the laser-heated sample.

## 5. Derivation and analysis of the partial DOS

The procedure to extract the partial DOS from the energy spectra of NRIXS experiments was introduced by Sturhahn et al. (1995). The pure phonon excitation spectra were obtained after the central elastic peak was subtracted from the measured energy spectra (Fig. 3) (Sturhahn et al., 1995). We measured the resolution function of the high-resolution monochromator with an energy bandwidth of 1 meV. The high-energy resolution of 1 meV is essential for deriving accurate Debye sound velocities ( $V_D$ ) from the PDOS (the Debye parabola is best constrained at the lower energy limit). The Lamb–Mössbauer factor, as well as the decomposition of the spectrum into individual phonon contributions, critically depends on the removal of the elastic peak. A quasi-harmonic model with well-defined phonon states and multiphonon contributions was used to derive the PDOS from the NRIXS energy spectra by using the PHOENIX software (Sturhahn et al., 1995; Sturhahn, 2000) (Fig. 4). The measured spectrum was decomposed to a one-phonon contribution, a two-phonon contribution, and higher order contributions. The multiphonon contributions were subtracted from the energy spectrum, and the remaining single-phonon contribution gives the phonon DOS (Sturhahn, 2000). As shown in Figure 4, the partial DOS are shifted to lower energies at 1400 K, indicating the softening of the lattice vibrations at high temperatures. The shift in the PDOS spectra of the nonmagnetic  $\text{Fe}_2\text{O}_3$  would naturally affect all derived thermodynamic and elastic parameters, allowing a better understanding of the temperature dependence of the NRIXS spectra. The NRIXS studies of iron in the bcc and fcc phases also reported an energy shift of the DOS and softening of the lattice vibrations under high temperatures (Chumakov et al., 1997; Shen et al., 2004).

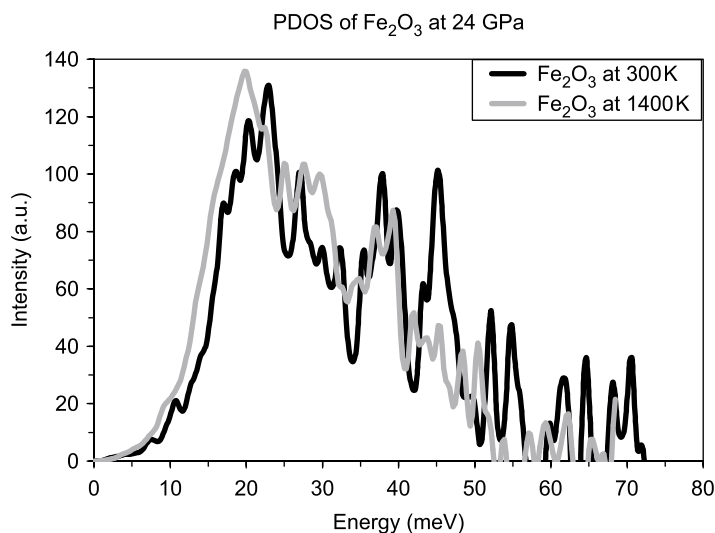


Figure 4. Partial DOS of  $\text{Fe}_2\text{O}_3$  at 24 ( $\pm 1.2$ ) GPa and 300 K (black curve) and 24 ( $\pm 1.2$ ) GPa and 1400 K ( $\pm 100$ ) (grey curve). Debye sound velocities are derived from parabolic fitting of the low-energy regime of the DOS in the range of 3.5–14 meV. The spectral features above  $\sim 55$  meV are just background noise.

Since the thermal EOS of  $\text{Fe}_2\text{O}_3$  is still unknown, we discuss here the general procedure of deriving the aggregate compressional wave velocity ( $V_P$ ), the shear wave velocity ( $V_S$ ), and the average shear modulus ( $G$ ) from the Debye sound velocity ( $V_D$ ) and the EOS. The value of  $V_D$  was derived from parabolic fitting of the low-energy slope of the PDOS in the range of 3.5–14 meV after applying a correction factor, the cube root of the ratio of the mass of the nuclear resonant isotope ( $^{57}\text{Fe}$ ) to the average atomic mass of the sample (Hu et al., 2003). While the obtained partial DOS gives only part of the lattice dynamics of the material, the low-energy portion of the partial DOS provides the bulk  $V_D$ . The method of extracting the  $V_D$  from partial DOS, based on the quasi-harmonic approximation, has been tested for different  $^{57}\text{Fe}$ -bearing materials with Debye-like low-frequency dynamics (Hu et al., 2003) and used to derive the sound velocities of Fe–Ni, Fe–Si, Fe–H, and Fe–S alloys under high pressures (Lin et al., 2003; Lin et al., 2004b; Mao et al., 2004). The vibrational kinetic energy ( $E_k$ ), zero-point energy ( $E_z$ ), vibrational heat capacity ( $C_{\text{vib}}$ ), vibrational entropy ( $S_{\text{vib}}$ ), and other thermodynamic and vibrational parameters were also calculated by integrating the partial DOS, which represent the contribution of the Fe sublattice (Table 1) (Sturhahn, 2000; Mao et al., 2001). These parameters are useful for testing theoretical calculations on Fe-containing materials under high pressures and high temperatures. In most applications, the resonant isotope ( $^{57}\text{Fe}$ ) is only one of the several constituents of the materials under investigation, and the quantities derived from the integration of the partial DOS only represent the contribution of the resonant isotope,  $^{57}\text{Fe}$ . These quantities may not be representative for the full thermodynamic behaviour of the sample, and theoretical calculations may be needed to complement experimental results.

The procedure for deriving aggregate  $V_P$ ,  $V_S$ , and  $G$  from the  $V_D$  and EOS parameters, namely the adiabatic bulk modulus ( $K_S$ ) and density ( $\rho$ ), has been described previously (Mao et al., 2001; Lin et al., 2003; Lin et al., 2004b; Struzhkin et al., 2004). The  $K_S$  and  $\rho$

Table 1. Elastic, vibrational, and thermodynamic parameters of  $\text{Fe}_2\text{O}_3$  at 24 GPa.

$T$ (K)	300	1400 (150)
$T_{D1}$ (K)	520 (60)	440 (440)
$T_{D2}$ (K)	453 (10)	404 (40)
$V_D$ (THz $\times$ (vol) $^{1/3}$ )	15.68 (0.64)	14.11 (0.03)
$E_k$ (meV/atom)	14.36 (0.67)	60.6 (1.1)
$D_{\text{av}}$ (N/m)	256 (28)	190 (13)
$f_{\text{LM}}$	0.8074 (0.0058)	0.3132 (0.0023)
$f_{\text{TM}, T=0}$	0.9275 (0.0016)	0.9191 (0.0006)
$E_z$ (meV/atom)	7.92 (0.52)	6.89 (0.21)
$C_{\text{vib}}$ ( $k_B$ /atom)	2.593 (0.082)	2.985 (0.045)
$S_{\text{vib}}$ ( $k_B$ /atom)	2.777 (0.064)	7.672 (0.085)

Lamb–Mössbauer factor,  $f_{\text{LM}}$ ; kinetic energy,  $E_k$ ; mean force constant,  $D_{\text{av}}$ ; Lamb–Mössbauer factor at  $T = 0$ ,  $f_{\text{TM}, T=0}$ ; kinetic energy at  $T = 0$ ,  $E_z$ ; vibrational specific heat,  $C_{\text{vib}}$ ; vibrational entropy,  $S_{\text{vib}}$ ; Boltzmann constant,  $k_B$ .  $T_{D1}$  is the Debye temperature calculated from the specific heat. The large error for the Debye temperature at 1400 K is typical because the specific heat approaches  $3k_B$ /atom and is very insensitive to the details of the PDOS.  $T_{D2}$  is the Debye temperature calculated from the Lamb–Mössbauer factor at 0 K. We note that these values only represent the contribution of the Fe sublattice. The Debye temperatures slightly decrease with increasing temperature.

of the material can be calculated using the Birch–Murnaghan EOS. The adiabatic bulk modulus at zero pressure ( $K_{0S}$ ) is calculated as:

$$K_{0S} = K_{0T}(1 + \alpha\gamma T), \quad (3)$$

where  $K_{0T}$  is the isothermal bulk modulus at zero pressure,  $\alpha$  is the thermal expansion coefficient,  $\gamma$  is the Grüneisen parameter, and  $T$  is temperature (300 K). The  $K_S$ ,  $\rho$ , and  $V_D$  are used to solve for the aggregate  $V_P$ ,  $V_S$ , and  $G$  by the following equations:

$$\frac{K_S}{\rho} = V_P^2 - \frac{4}{3}V_S^2 \quad (4)$$

$$\frac{G}{\rho} = V_S^2 \quad (5)$$

$$\frac{3}{V_D^3} = \frac{1}{V_P^3} + \frac{2}{V_S^3}. \quad (6)$$

As shown in the above equations,  $V_S$  is relatively insensitive to the differences in the EOS data. Therefore, the NRIXS technique is particular good at constraining  $V_S$  with a precise measurement of  $V_D$ . However, the use of the EOS parameters ( $K_S$ ,  $\rho$ ) introduces relatively high uncertainties in the aggregate  $V_P$ . Although previous NRIXS studies on the temperature dependence of the DOS of iron to 920 K did not show any evident deviation from the harmonic approximation (Chumakov et al., 1997; Shen et al., 2004), the potential deviation of the Debye-like behaviour of the partial DOS at higher temperatures would also affect the accuracy of deriving the sound velocities from the low-energy region of the partial DOS.

## 6. SMS spectra under high pressures and temperatures

In the SMS experiments, the time spectrum is a collection of events that reveal the time span between the arrival of the synchrotron radiation pulses and the arrival of scattered photons. The time spectra were recorded by an APD in the forward direction (Figs 1 and 2). Time spectra of  $\text{Fe}_2\text{O}_3$  have been collected up to 24 GPa and 1400 K in steps of  $\sim 100$  K (Fig. 5a–b). Time spectra at 10 and 24 GPa upon laser heating reveal that  $\text{Fe}_2\text{O}_3$  undergoes a magnetic to nonmagnetic transition at 900 ( $\pm 100$ ) K and 1000 ( $\pm 100$ ) K, respectively, from a room-temperature magnetic state to a high-temperature nonmagnetic state (Fig. 5a, b). This magnetic transition is found to be reversible with temperature. Since the Néel temperature of hematite is 956 K at ambient pressure, our results show that the Néel temperature remains unchanged with the present accuracy up to 24 GPa. A magnetic-to-nonmagnetic transition in hematite has also been observed under high pressures at  $\sim 50$  GPa and 300 K; although, the magnetic breakdown is reported to be connected with a first-order structural transition (Pasternak et al., 1999; Badro et al., 2002). The time spectra are evaluated with the CONUSS programs to permit derivation of magnetic hyperfine parameters (Sturhahn, 2000) (Fig. 6). The magnetic hyperfine field is 52.20 T ( $\pm 0.02$ ) at 24 GPa and 300 K, a typical value of the hyperfine field for ionic ferric oxide bonding, consistent with previous Mössbauer studies (Pasternak et al., 1999).

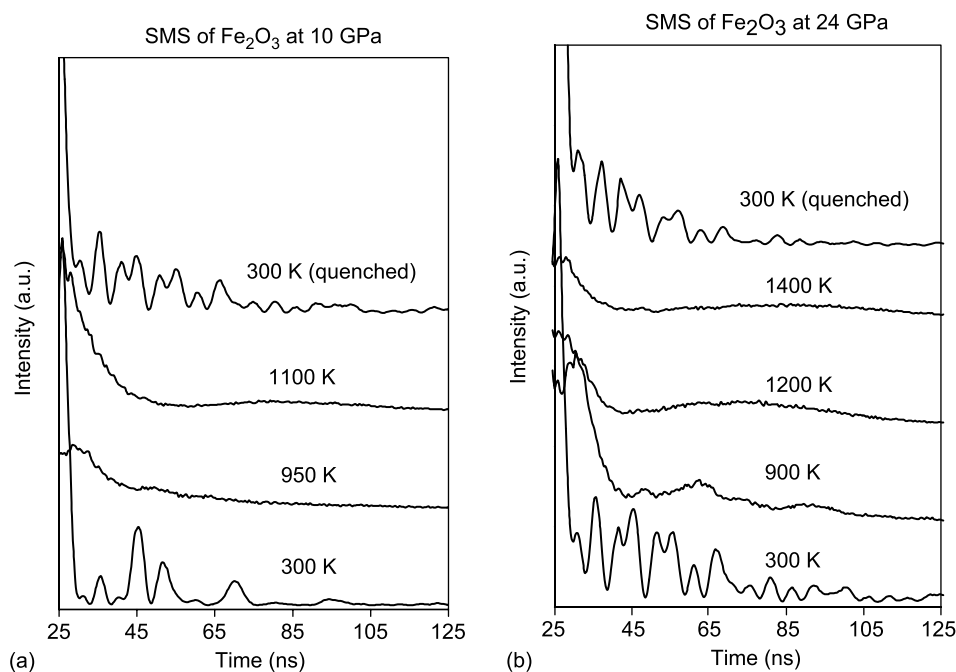


Figure 5. Representative time spectra of the SMS of  $\text{Fe}_2\text{O}_3$  at 10 GPa (a) and 24 GPa (b) upon laser heating. Temperatures were determined from the energy spectra based on the detailed balance principle. The decay time is dictated by the nuclear lifetime of the  $^{57}\text{Fe}$  nuclei in  $\text{Fe}_2\text{O}_3$ . Oscillations in the time spectra are observed that originate from the nuclear-level splitting (Sturhahn, 2004), whereas the flat feature indicates a nonmagnetic state. The spectra were collected at a temperature step of  $\sim 100$  K from 300 to 1400 K.

At approximately 1100 K, a magnetic-to-nonmagnetic transition occurs; the magnetic component is highly reduced to approximately 5% at 1100 K. A pure quadrupole spectrum is observed at 1400 K. We note that the absolute temperature measurement is also very useful in the SMS study at temperatures below 1000 K, where the spectroradiometric method is limited due to the weak thermal emission. The sample temperature can be directly determined from the energy spectra, whereas the time spectra reveal magnetic ordering within the sample.

## 7. Conclusions

Here we have interfaced the LHDAC system with the NRIXS and SMS techniques to explore particular physical properties of  $^{57}\text{Fe}$ -containing materials as they exist deep in the Earth's interior. The SMS spectra and the partial DOS of  $\text{Fe}_2\text{O}_3$  have been measured with these techniques up to 24 GPa and 1400 K, providing rich information on the physical properties of the sample under high pressures and temperatures. The detailed balance principle applied to the NRIXS energy spectra provides absolute temperatures

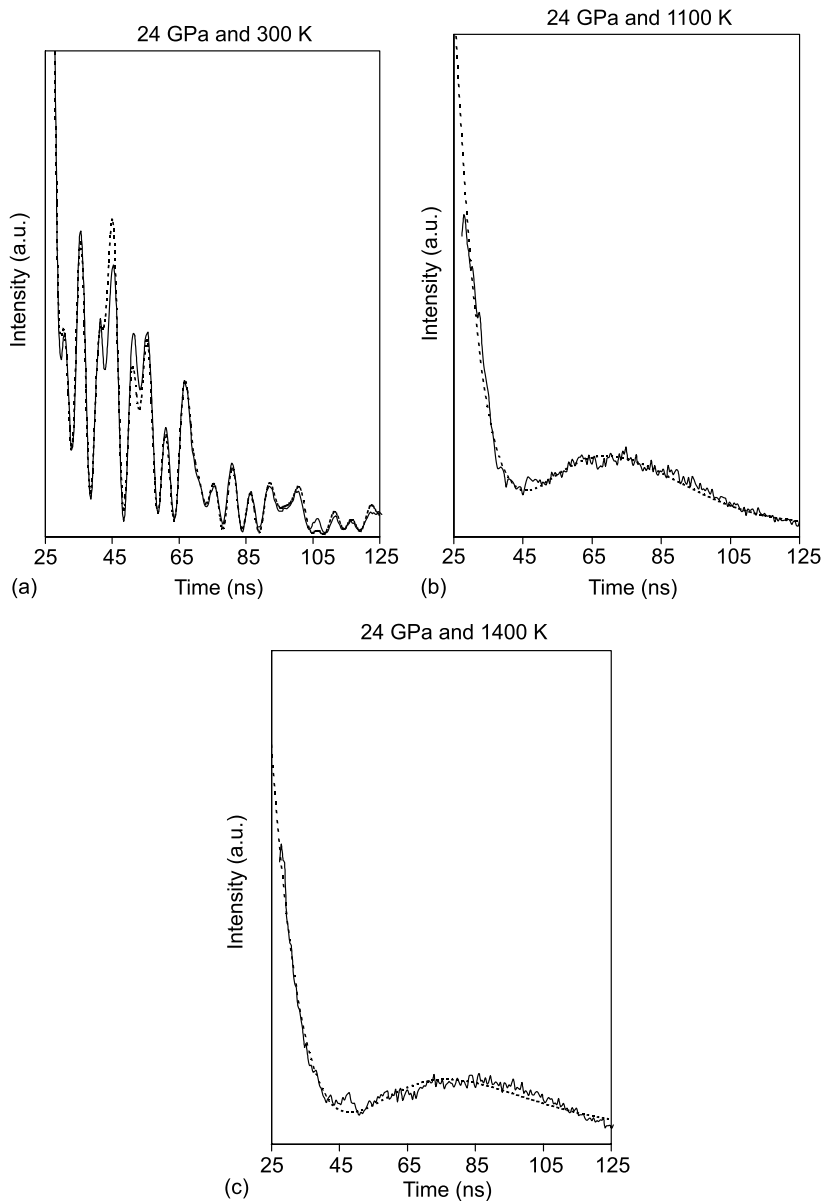


Figure 6. The SMS spectra at 300 K (a), 1100 K (b), and 1400 K (c) are evaluated by CONUSS programs to permit derivation of magnetic hyperfine parameters (Sturhahn, 2000). The magnetic hyperfine field is 52.20 T ( $\pm 0.02$ ) at 24 GPa and 300 K, a typical value of the hyperfine field for ionic ferric oxide bonding, which is also consistent with previous Mössbauer studies (Pasternak et al., 1999). At approximately 1100 K, a magnetic-to-nonmagnetic transition occurs; the magnetic component is highly reduced to approximately 5% at 1100 K. A pure quadrupole spectrum is observed at 1400 K. Solid curves: experimental time spectra; dashed curves: time spectra calculated from the CONUSS programs.

of the laser-heated sample. Time spectra of the SMS can be used to determine magnetic phase diagrams under high pressures and temperatures. The application of the LHDAC technique with NRIXS and SMS provides a new arsenal of probes to study the magnetic, vibrational, elastic, and thermodynamic properties of  $^{57}\text{Fe}$ -containing materials, such as Fe, Fe alloys,  $(\text{Mg,Fe})\text{O}$ , and  $(\text{Mg,Fe})\text{SiO}_3$  as they exist in the Earth's interior. The SMS technique is based on coherent elastic scattering from nuclear resonances in the forward direction. For a given experimental situation, the scattering intensity will decrease if the probability for recoilless absorption of the X-rays by the nuclei is reduced. The probability for recoilless absorption is also known as the Lamb–Mössbauer factor, and, more importantly, it vanishes for liquids and gases. In contrast to diffraction technique, the SMS signal only depends on the solid state of the sample but not on spatial order. Therefore, our techniques can also be used to measure the melting curves of iron-containing materials. These studies also provide useful parameters for testing theoretical calculations on Fe-containing materials under high pressures and temperatures.

### Acknowledgements

This work and use of the APS are supported by US Department of Energy, Basic Energy Sciences, Office of Science under contract No. W-31-109-ENG-38, and the State of Illinois under HECA. We thank GSECARS, APS for the use of the ruby fluorescence system. We also thank E.E. Alp, D. Errandonea, S.-K. Lee, V. Struzhkin, M. Hu, D.L. Heinz, G. Steinle-Neumann, R. Cohen, J. Burke, V. Prakapenka, M. Rivers, S. Hardy, S. Jacobsen, and J.M. Jackson for their help and discussions. Work at Carnegie was supported by DOE/BES, DOE/NNSA (CDAC grant DE-FC03-03NA00144), NASA, NSF, and the W.M. Keck Foundation.

### References

- Alp, E.E., Sturhahn, W., Toellner, T.S., 2001. Lattice dynamics and inelastic nuclear resonant x-ray scattering. *J. Phys.: Condens. Matter* 13, 7645–7658.
- Badro, J., Fiquet, G., Struzhkin, V.V., Somayazulu, M., Mao, H.K., Shen, G., Le Bihan, T., 2002. Nature of the high-pressure transition in  $\text{Fe}_2\text{O}_3$  hematite. *Phys. Rev. Lett.* 89, 205504.
- Bassett, W.A., 2001. The birth and development of laser heating in diamond anvil cells. *Rev. Sci. Instrum.* 72, 1270–1272.
- Boehler, R., 1986. The phase diagram of iron to 430 kbar. *Geophys. Res. Lett.* 13, 1153–1156.
- Boehler, R., Chopelas, A., 1991. A new approach to laser heating in high pressure mineral physics. *Geophys. Res. Lett.* 18, 1147–1150.
- Chumakov, A.I., Rüffer, R., Baron, A.Q.R., Grünsteudel, H., Grünsteudel, H.F., 1997. Temperature dependence of nuclear inelastic absorption of synchrotron radiation in  $\alpha$ - $^{57}\text{Fe}$ . *Phys. Rev. B* 54, R9596–R9599.
- Dewaele, A., Figuet, G., Andrault, D., Hausermann, D., 2000. P–V–T equation of state of periclase from synchrotron radiation measurements. *J. Geophys. Res.* 105, 2869–2877.
- Gieffers, H., Lübbers, R., Rupprecht, K., Wortmann, G., Alfé, D., Chumakov, A.I., 2002. Phonon spectroscopy of oriented hcp iron. *High Pressure Res.* 22, 501–506.
- Hastings, J.B., Siddons, D.P., van Bürcck, U., Hollatz, R., Bergmann, U., 1991. Mössbauer spectroscopy using synchrotron radiation. *Phys. Rev. Lett.* 66, 770–773.

- Heinz, D.L., Jeanloz, R., 1987. Temperature measurements in the laser-heated diamond cell. In: Manghnani, M.H., Syono, Y. (Eds), High-Pressure Research in Mineral Physics. Terra Scientific Publishing Company (TERRAPUB), Tokyo/American Geophysical Union, Washington, DC, pp. 113–127.
- Hemley, R.J., Mao, H.K., Gramsch, S.A., 2000. Pressure-induced transformations in deep mantle and core minerals. *Mineral. Mag.* 64, 157–184.
- Hu, M., Sturhahn, W., Toellner, T.S., Mannheim, P.D., Brown, D.E., Zhao, J., Alp, E.E., 2003. Measuring velocity of sound with nuclear resonant inelastic x-ray scattering. *Phys. Rev. B* 67, 094304.
- Jackson, J.M., Sturhahn, W., Shen, G., Zhao, J., Hu, M.Y., Errandonea, D., Bass, J.D., Fei, Y., 2005. A synchrotron Mössbauer spectroscopy study of (Mg,Fe)SiO<sub>3</sub> perovskite up to 120 GPa. *Am. Miner.*, 90, 199–205.
- Lazor, P., Shen, G., Saxena, S.K., 1993. Laser-heated diamond anvil cell experiments at high pressure: melting curve of nickel up to 700 kbar. *Phys. Chem. Miner.* 20, 86–90.
- Lin, J.F., Struzhkin, V.V., Sturhahn, W., Huang, E., Zhao, J., Hu, M.Y., Alp, E., Mao, H.K., Boctor, N., Hemley, R.J., 2003. Sound velocities of iron–nickel and iron–silicon alloys in the Earth's core. *Geophys. Res. Lett.* 30, 2112.
- Lin, J.F., Santoro, M., Struzhkin, V.V., Mao, H.K., Hemley, R.J., 2004a. *In situ* high pressure-temperature Raman spectroscopy technique with laser-heated diamond anvil cells. *Rev. Sci. Instrum.* 75, 3302–3306.
- Lin, J.F., Fei, Y., Sturhahn, W., Zhao, J., Mao, H.K., Hemley, R.J., 2004b. Magnetic transition and sound velocities of Fe<sub>3</sub>S at high pressure. *Earth Planet. Sci. Lett.* 226, 33–40.
- Lin, J.F., Sturhahn, W., Zhao, J., Shen, G., Mao, H.K., Hemley, R.J., 2004c. Absolute temperature measurement in a laser-heated diamond anvil cell. *Geophys. Res. Lett.* 31, L14611.
- Lübbbers, R., Wortmann, G., Grünsteudel, H.F., 1999a. High-pressure studies with nuclear scattering of synchrotron radiation. *Hyperfine Interact.* 123/124, 529–559.
- Lübbbers, R., Pleines, M., Hesse, H.J., Wortmann, G., Grünsteudel, H.F., Ruffer, R., Leupold, O., Zukrowski, J., 1999b. Magnetism under high pressure studied by <sup>57</sup>Fe and <sup>151</sup>Eu nuclear scattering of synchrotron radiation. *Hyperfine Interact.* 120/121, 49–58.
- Lübbbers, R., Grünsteudel, H.F., Chumakov, A.I., Wortmann, G., 2000. Density of phonon states in iron at high pressure. *Science* 287, 1250–1253.
- Mao, H.K., Bell, P.M., Shaner, J.W., Steinberg, D.J., 1978. Specific volume measurements of Cu, Mo, Pd, and Ag and calibration of the ruby R<sub>1</sub> fluorescence pressure gauge from 0.06 to 1 Mbar. *J. Appl. Phys.* 49, 3276–3283.
- Mao, H.K., Xu, J., Struzhkin, V.V., Shu, J., Hemley, R.J., Sturhahn, W., Hu, M.Y., Alp, E.E., Vocadlo, L., Alfé, D., Price, G.D., Gillan, M.J., Schwoerer-Böhning, M., Häusermann, D., End, P., Shen, G., Giefers, H., Lübbbers, R., Wortmann, G., 2001. Phonon density of states of iron up to 153 gigapascals. *Science* 292, 914–916.
- Mao, W.L., Sturhahn, W., Heinz, D.L., Mao, H.K., Shu, J., Hemley, R.J., 2004. Nuclear resonant x-ray scattering of iron hydride at high pressure. *Geophys. Res. Lett.* 31, L15618.
- Ming, L.C., Bassett, W.A., 1974. Laser heating in the diamond anvil press up to 2000°C sustained and 3000°C pulsed at pressures up to 260 kilobars. *Rev. Sci. Instrum.* 45, 1115–1118.
- Pasternak, M.P., Rozenberg, G.Kh., Machavariani, G.Yu., Naaman, O., Taylor, R.D., Jeanloz, R., 1999. Breakdown of the Mott–Hubbard state in Fe<sub>2</sub>O<sub>3</sub>: a first-order insulator-metal transition with collapse of magnetism at 50 GPa. *Phys. Rev. Lett.* 82, 4663–4666.
- Pasternak, M.P., Rozenberg, G.Kh., Xu, W.M., Taylor, R.D., 2004. Effect of very high pressure on the magnetic state of transition metal compounds. *High Pressure Res.* 24, 33–43.
- Ruffer, R., Chumakov, A.I., 2000. Nuclear inelastic scattering. *Hyperfine Interact.* 128, 255–272.
- Rupprecht, K., Friedmann, T., Gieffers, H., Wortmann, G., Doyle, B., Zukrowski, J., 2002. High-pressure/high-temperature NFS study of magnetism in LuFe<sub>2</sub> and ScFe<sub>2</sub>. *High Pressure Res.* 22, 189–194.
- Santoro, M., Lin, J.F., Mao, H.K., Hemley, R.J., 2004. *In situ* high P–T Raman spectroscopy and laser heating of carbon dioxide. *J. Chem. Phys.* 121, 2780–2787.
- Seto, M., Yoda, Y., Kikuta, S., Zhang, X.W., Ando, M., 1995. Observation of nuclear resonant scattering accompanied by phonon excitation using synchrotron radiation. *Phys. Rev. Lett.* 74, 3828–3831.
- Shen, G., Mao, H.K., Hemley, R.J., Duffy, T.S., Rivers, M.L., 1998. Melting and crystal structure of iron at high pressures and temperatures. *Geophys. Res. Lett.* 25, 373–376.
- Shen, G., Rivers, M.L., Wang, Y., Sutton, S.R., 2001. Laser heated diamond cell system at the Advanced Photon Source for *in situ* x-ray measurements at high pressure and temperature. *Rev. Sci. Instrum.* 72, 1273–1282.

- Shen, G., Sturhahn, W., Alp, E.E., Zhao, J., Toellner, T.S., Prakapenka, V.B., Meng, Y., Mao, H.K., 2004. Phonon density of states in iron at high pressures and high temperatures. *Phys. Chem. Miner.* 31, 353–359.
- Struzhkin, V.V., Mao, H.K., Mao, W.L., Hemley, R.J., Sturhahn, W., Alp, E.E., L'Abbe, C., Hu, M.Y., Errandonea, D., 2004. Phonon density of states and elastic properties of Fe-based materials under compression. *Hyperfine Interact.* 153, 3–15.
- Sturhahn, W., Toellner, T.S., Alp, E.E., Zhang, X., Ando, M., Yoda, Y., Kikuta, S., Seto, M., Kimball, C.W., Dabrowski, B., 1995. Phonon density of states measured by inelastic nuclear resonant scattering. *Phys. Rev. Lett.* 74, 3832–3835.
- Sturhahn, W., Alp, E.E., Toellner, T.S., Hession, P., Hu, M., Sutter, J., 1998. Introduction to nuclear resonant scattering with synchrotron radiation. *Hyperfine Interact.* 113, 47–58.
- Sturhahn, W., 2000. CONUSS and PHOENIX: Evaluation of nuclear resonant scattering data. *Hyperfine Interact.* 125, 149–172.
- Sturhahn, W., 2004. Nuclear resonant spectroscopy. *J. Phys.: Condens. Matter* 16, S497–S530.